ARTICLE

JAAS
www.rsc.org/jaas

Nanosecond laser ablation of Cu: modeling of the expansion in He background gas, and comparison with expansion in vacuum†

Annemie Bogaerts* and Zhaoyang Chen

University of Antwerp, Department of Chemistry, Universiteitsplein 1, B-2610 Wilrijk-Antwerp, Belgium. E-mail: annemie.bogaerts@ua.ac.be

Received 26th February 2004, Accepted 15th June 2004
First published as an Advance Article on the web 17th August 2004

A model is developed for nanosecond laser ablation of a Cu target, followed by the expansion of the Cu vapor in He background gas at 1 atm. Typical calculation results include the temperature distribution in the target, information about target melting and vaporization, the density profiles of the Cu vapor and the He background gas in front of the target, as well as the velocity and temperature distributions in the plume. Comparison is made with results calculated for expansion in vacuum. It is found that the vapor plume pushes the background gas away from the target, but at the same time, the vapor plume is much more confined in space compared with expansion in vacuum. Indeed, the plume expansion velocity is much lower in the case of a background gas. Also, the plume temperature is much lower, which is attributed, among other things, to the cooling effect of the background gas.

1. Introduction

Laser ablation (LA) is applied in several fields: among others, pulsed laser deposition,[1] nanoparticle manufacturing,[2] micromachining,[3] surgery,[4] as well as for various chemical analysis techniques, such as matrix assisted laser desorption ionization (MALDI),[5] laser-induced breakdown spectrometry (LIBS),[6] and as a sample introduction method for the inductively coupled plasma (ICP).[7–10] In spite of the many applications, the exact processes taking place during and after LA are not yet fully understood, and there are still a lot of open questions, for instance:

- Why is the crater shape after LA so different for different materials (*e.g.*, metals *versus* geological materials)?
- How are the processes, taking place during and after LA, affected by the background gas (gas pressure, kind of gas: helium, argon, air …) and the laser parameters (wavelength, pulse duration …)?
- Why does LA-ICP-MS suffer from fractionation (*i.e.*, non-stoichiometric sampling)? This is reported[10] to be attributed to the formation of particles with varying sizes, *i.e.*, small particles can be easily transported to the ICP, and atomized/excited/ionized within the ICP, in comparison with larger particles. Hence, the next question arises: which processes are responsible for the formation of particles, and why are different groups of particles observed, with different sizes?
- How is the particle formation affected by LA parameters (laser wavelength, pulse duration, He or Ar background gas …)?

In order to provide answers to these questions, a better understanding of the various mechanisms taking place during and after LA is required. For this reason, we aim at developing a comprehensive model to describe LA, with the main emphasis on the application as a sample introduction method for the ICP. However, the model will be built in a flexible way, so that it can be interesting for other applications as well. The entire picture of processes taking place during and after LA is very complicated, and cannot be described with one single model. Hence, we started with a "simple" model for LA of a Cu target, with expansion in vacuum, and this model will be gradually improved and extended in the coming years to describe the real situation, *i.e.*, expansion in a background gas at 1 atm, including the formation of particles by various mechanisms (*e.g.*, condensation in the expanding vapor plume, liquid splashing of the molten target …), and also applied to a range of different LA conditions (*e.g.*, nanosecond *versus* femtosecond pulsed LA, metals *versus* geological materials …), so that finally, decent answers can be given to the questions arising from the applications.

In previous work,[11] we have already developed a model to describe the LA of a Cu target in vacuum. The model deals with (i) laser-solid interaction, yielding heating, melting and vaporization of the Cu target, (ii) expansion of the evaporated Cu material in vacuum, (iii) plasma formation in the evaporated plume, and (iv) plasma shielding of the incoming laser light. Results of this model included the temperature distribution in the target, the depth of melting, the vaporization rate, the density, velocity and temperature of the evaporated material plume, as well as the fraction and density of Cu^0 atoms, Cu^+ and Cu^{2+} ions in the plasma plume, all as a function of position (in the target, or in the plume) and as a function of time during and after the laser pulse.[11]

However, as mentioned, this model was applied to LA in vacuum, whereas LA as sample introduction method for the ICP occurs in an airtight ablation chamber that is flushed with a carrier gas (usually He or Ar), to transport the ablated material into the ICP. Consequently, the expansion of the evaporated material takes place in a background gas at 1 atm, instead of in vacuum. This makes the modeling much more complicated, because one has to consider not only the evaporated material, but also the background gas, and interactions between both. In the present paper we focus on this step in the model, *i.e.*, the description of LA of a Cu target, followed by expansion in a background gas.

In spite of the fact that there exist quite a lot of papers in the literature, describing models for LA, these models mainly focus on one aspect of the entire process (*e.g.*, laser–solid interaction, or plume expansion, or plasma formation), or they consider expansion in vacuum or in a low pressure background gas (100 Pa or lower). For a detailed overview of the different modeling approaches of LA, we refer to ref. 11. We are aware of only one set of papers that describe the plume expansion in 1 atm, using a hydrodynamic model with two distinct species (material plume and background gas) and describing interactions between them.[12–14] However, the authors only consider

† Presented at the 2004 Winter Conference on Plasma Spectrochemistry, Fort Lauderdale, Florida, January 5–10, 2004.

DOI: 10.1039/b402946a

a very low laser irradiance ($\sim 10^4$–10^5 W cm^{-2}). In our paper, we present a model that describes LA with expansion in 1 atm He gas, with a two-components hydrodynamic model, which applies to typical LA conditions used as sample introduction method for the ICP (*i.e.*, laser irradiance of the order of 10^8–10^9 W cm^{-2}).

2. Description of the model

The model is subdivided in three parts, describing the individual mechanisms:

(a) laser–solid interaction, yielding heating, melting and vaporization of the material;

(b) expansion of the material plume in a background gas at 1 atm;

(c) formation of a plasma in the material plume, and plasma shielding of the incoming laser light.

We will explain these mechanisms here in a bit more detail.

2.1. Laser–solid interaction: target heating, melting and vaporization

When the laser is focused on the solid target the temperature at the surface will rise, and eventually the target can melt, and even vaporize. The temperature distribution inside the target is calculated with a one-dimensional heat conduction equation. This part of the model is exactly the same as presented in ref. 11. Hence, all details can be found in that paper. The output of this model includes the temperature distribution in the target, the melt depth, the evaporation rate and evaporation depth, as well as the vapor density, velocity and temperature at the surface, which are used as input (*i.e.*, boundary condition) in the second part of the model (see below).

2.2. Expansion of the evaporated material in 1 atm He

The Euler equations of hydrodynamics, expressing the conservation of mass density, momentum and energy density during the expansion in vacuum, as explained in ref. 11, have to be extended to take into account the effect of the background gas. For a binary mixture (Cu vapor and He), in the one-dimensional case, the conservation equations are the following Navier–Stokes equations:

$$\frac{\partial \rho}{\partial t} + \frac{\partial}{\partial x}(\rho v) = 0 \tag{1}$$

$$\frac{\partial \rho_v}{\partial t} + \frac{\partial}{\partial x}(\rho_v v) = \frac{\partial}{\partial x}\left(\rho D_{mix} \frac{\partial}{\partial x}\omega_v\right) \tag{2}$$

$$\frac{\partial(\rho v)}{\partial t} = -\frac{\partial}{\partial x}(\rho v^2 + p) + \frac{4}{3}\frac{\partial}{\partial x}\left(\eta_{mix}\frac{\partial v}{\partial x}\right) \tag{3}$$

$$\begin{aligned}\frac{\partial}{\partial t}\left[\rho\left(E+\frac{1}{2}v^2\right)\right] &= -\frac{\partial}{\partial x}\left[\rho\left(E+\frac{1}{2}v^2+\frac{p}{\rho}\right)v\right] + \frac{\partial}{\partial x}\left[\kappa_{mix}\frac{\partial T}{\partial x}\right] \\ &+ \frac{\partial}{\partial x}\left[(H_v - H_b)\rho D_{mix}\frac{\partial \omega_v}{\partial x}\right] + \frac{\partial}{\partial x}\left[\frac{4}{3}\eta_{mix} v \frac{\partial v}{\partial x}\right] + \alpha_{IB} I_{laser} - \varepsilon_{rad}\end{aligned} \tag{4}$$

Here, ρ stands for the total mass density of the binary mixture, which is the sum of the vapor mass density (ρ_v) and background gas mass density (ρ_b). ω_v is the vapor mass density fraction: $\omega_v = \rho_v/\rho$. v is the flow velocity of the binary mixture, p is the total pressure of this mixture, E is the internal energy per unit mass, T is the temperature, and H_v and H_b stand for the enthalpy per unit mass of the vapor and background gas, respectively. Further, D_{mix} is the binary diffusion coefficient of the vapor–background gas mixture, κ_{mix} is the thermal conductivity and η_{mix} is the viscosity of the binary mixture. Finally, I_{laser} denotes the laser intensity, α_{IB} is the absorption coefficient due to inverse Bremsstrahlung (IB), and ε_{rad} is the radiation power loss emitted in the Bremsstrahlung process.

Eqn. (1) describes the conservation of total mass density, whereas eqn. (2) gives the conservation of vapor mass density. The right-hand side denotes the binary diffusion of the vapor and the background gas in the binary mixture. The binary diffusion coefficient of the vapor–background gas mixture is defined as:[15]

$$D_{mix} = \frac{2}{3}\left(\frac{k}{\pi}\right)^{3/2}\left(\frac{1}{2m_v}+\frac{1}{2m_b}\right)^{1/2}\frac{T^{3/2}}{p\left(\frac{d_v+d_b}{2}\right)^2}$$

where k is the Boltzmann constant, T and p are the temperature and pressure, and m and d stand for the mass and diameter of vapor atoms (v) and background gas atoms (b), respectively. Note that during the laser pulse, when the laser irradiance is high, the Cu vapor pressure at the contact surface between the Cu vapor and the ambient gas is much larger than the pressure of the undisturbed region. In this period, the binary diffusion may not be significant. When the temperature of the plume increases, the plume may be ionized to some degree, and when the plasma shielding is strong, the laser irradiance arriving at the target surface decreases very quickly, so that the amount of evaporated material from the target drops as well. From this moment on, the plume expansion will slow down due to the lack of source of energy and material, and the contact surface between the Cu vapor and ambient gas will be smeared out and, consequently, binary diffusion should be taken into account.

Eqn. (3) describes the conservation of total momentum. The first term at the right-hand side stands for the change in momentum as a result of kinetic energy gradient and pressure gradient. Assuming that the binary gas mixture follows the ideal gas law, the total pressure can be expressed as:

$$p = (1+x_{e,v})\frac{\rho_v k T}{m_v} + (1+x_{e,b})\frac{\rho_b k T}{m_b}$$

where $x_{e,v}$ and $x_{e,b}$ denote the fraction of electrons resulting from ionization of the vapor and of the background gas, respectively.

The second term on the right-hand side of eqn. (3) is the viscosity term giving rise to a change in momentum (friction force). The viscosity for the binary mixture is defined from the viscosity of the individual components (vapor and background gas), with the semi-empirical formula of Wilke:[15]

$$\eta_{mix} = \sum_{i=1}^{n}\frac{x_i\eta_i}{\sum_{j=1}^{n} x_j\Phi_{ij}} = \frac{x_v\eta_v}{x_v\Phi_{vv}+x_b\Phi_{vb}} + \frac{x_b\eta_b}{x_v\Phi_{bv}+x_b\Phi_{bb}}$$

where x_i and η_i are the number density fraction and the viscosity of the vapor (v) and background gas (b) atoms, respectively, and Φ_{ij} is a dimensionless quantity:

$$\Phi_{ij} = \frac{1}{\sqrt{8}}\left(1+\frac{m_i}{m_j}\right)^{-1/2}\left[1+\left(\frac{\mu_i}{\mu_j}\right)^{1/2}\left(\frac{m_j}{m_i}\right)^{1/4}\right]^2$$

Note that Φ_{ij} is equal to 1 for i = j. The viscosity of the individual components is calculated from the kinetic gas theory formula:

$$\eta_i = \frac{1}{\pi d_i^2}\sqrt{\frac{m_i k T}{\pi}}$$

with d_i and m_i being the diameter and mass of the atom (vapor or background gas).

Finally, eqn. (4) denotes the conservation of total energy density, *i.e.*, the sum of internal energy density (ρE, thermal motion of the gas) and kinetic energy density of the flow ($\rho v^2/2$, with v being the flow velocity). The internal energy density of the binary gas mixture can be expressed based on the ideal

gas law:

$$\rho E = \frac{\rho_v}{m_v}\left[\frac{3}{2}(1+x_{e,v})kT + IP_{Cu1}x_{Cu1} + (IP_{Cu1}+IP_{Cu2})x_{Cu2}\right] + \frac{\rho_b}{m_b}\left[\frac{3}{2}(1+x_{e,b})kT + IP_{He1}x_{He1}\right]$$

where $x_{e,v}$ and $x_{e,b}$ have been explained above, x_{Cu1}, x_{Cu2} and x_{He1} stand for the fraction of Cu^+, Cu^{2+} and He^+ ions in the gas mixture, and IP_{Cu1}, IP_{Cu2} and IP_{He1} denote the first and second ionization potential of Cu and the first ionization potential of He, respectively. These extra terms, and the factors $(1 + x_{e,v/b})$ are needed to account for the partial ionization of the vapor and background gas (see below, section 2.3).

The first term on the right-hand side of eqn. (4) denotes the spatial gradient in internal energy, flow energy and pressure. The second term gives the heat flux due to thermal conduction. The thermal conductivity of the binary gas mixture is also defined from the thermal conductivity of the individual components, with the same semi-empirical formula as for the viscosity (see above), and the thermal conductivity of the vapor and background gas atoms is defined as:[15]

$$\kappa_i = \frac{1}{d_i^2}\sqrt{\frac{k^3 T}{\pi^3 m_i}}$$

The third term stands for the spatial gradient in composition of the binary gas mixture (*i.e.*, fraction of vapor number density), yielding a change in energy if the enthalpy values of vapor and background gas are different. The fourth term is related to the work done by the viscous force. The fifth term denotes the energy gain due to absorption of laser energy in the plume (see below, section 2.3), and the last term describes the amount of energy emitted by the binary gas mixture per unit volume and time, in the Bremsstrahlung process, which means a loss for the internal energy. It can be expressed by:[11]

$$\varepsilon_{rad} = \left(\frac{2\pi kT}{3m_e}\right)^{1/2}\frac{32\pi e^6}{3hm_e c^3} n_e \sum_i Z_i^2 n_i g_i$$

where m_e and e are the electron mass and charge, respectively, c is the velocity of light, n_e is the electron density, n_i and Z_i denote the density and charge of the ions (Cu^+, Cu^{2+} and He^+), and g_i stands for the Gaunt factor, which can be assumed to be equal to 1.

It is clear that the four conservation equations contain many terms with second order derivatives, and several non-linear terms. Therefore, solving these equations is a difficult numerical problem. We have tried several methods,[16] such as the Lax–Friedrichs method and the explicit Euler upwinding method. However, these methods are first-order accurate and highly dissipative, hence they could not treat the mass conservation in a correct way. The Godunov scheme, which was used in the case of LA in vacuum,[11] appeared not to be suitable for the solution of the two-component hydrodynamic equations. Finally, we relied on the MacCormack method with second order accuracy. In this case, the mass conservation is correctly accounted for. However, this method appears to suffer from stability problems. Therefore, special care has to be taken with the boundary conditions, the time-step and the spatial grid, in order to keep the calculations stable. However, this method still appears to become unstable when the ionization degree in the plume is too high, so that the calculation results presented in this paper are, in practice, limited to not too high laser irradiance (see below).

It was mentioned above (section 2.1) that the vapor density, velocity and temperature at the surface were used as boundary conditions for the conservation equations of the expansion process. This is, however, not completely true. Indeed, for high background gas pressure (*e.g.*, 1 atm), a narrow Knudsen layer in front of the target has to be taken into account. Within this Knudsen layer, the vapor flow is not in local thermodynamic equilibrium, and it does not obey the Maxwellian distribution.[17] In the model, this layer is treated as a gas dynamic discontinuity and some approximate equations to describe the jump conditions for the density and temperature are applied:[17]

$$\frac{T}{T_s} = \left[\sqrt{1+\pi\left(\frac{\gamma-1}{\gamma+1}\frac{m}{2}\right)^2} - \sqrt{\pi}\frac{\gamma-1}{\gamma+1}\frac{m}{2}\right]^2$$

$$\frac{\rho_v}{\rho_{v,s}} = \sqrt{\frac{T_s}{T}}\left[\left(m^2+\frac{1}{2}\right)e^{m^2}\mathrm{erfc}(m) - \frac{m}{\sqrt{\pi}}\right] + \frac{1}{2}\frac{T_s}{T}\left[1-\sqrt{\pi}me^{m^2}\mathrm{erfc}(m)\right]$$

Here, T_s and $\rho_{v,s}$ are the temperature and vapor density at the target surface, and T and ρ_v are the temperature and vapor density beyond the Knudsen layer. Further, γ is the ratio of specific heats ($\gamma = C_p/C_v = 5/3$ for a monoatomic gas), and m is a number related to the Mach number M, through $m = M\sqrt{\frac{\gamma}{2}}$ The value of m is related to the vapor velocity (v) and temperature (T) just beyond the Knudsen layer, *via*:

$$m = v\Big/\sqrt{2RT}$$

Note, however, that this temperatue depends exactly on m (see equations above). Hence, the Knudsen layer analysis provides no information about the value of m. Therefore, m needs to be determined in an iterative way, based on the target temperature as well as the energy balance at the surface (*i.e.*, absorbed incident laser radiation *versus* conductive heat loss to the surroundings and latent heat carried away by vapor leaving the Knudsen layer (*i.e.*, evaporation)). For more information about this Knudsen layer theory, we refer to ref. 17.

2.3. Plasma formation and laser absorption in the plasma

Plasma formation in the plume will take place when the temperature of the evaporated material, and hence of the binary gas mixture, is very high, and thus the Cu and He atoms will be ionized. Since many collisions take place between the various species, the plasma is considered in local thermal equilibrium (LTE), which implies that in a sufficiently small region of the gas mixture, thermal equilibrium is established between the electrons, ions and neutrals, so that they are characterized by a common temperature. Moreover, the ionization degree can then be described with Saha equations.

The model for the plasma formation is very similar to the one described in ref. 11, except that now an extra Saha equation is added for the He^+ ions, and that the fraction of He^0 atoms and He^+ ions also should be included in the equations for conservation of matter and charge. This leads to the following equations:

$$\frac{x_{Cu1}}{x_{Cu0}} = \frac{1}{n_e}\left(\frac{2\pi m_e kT}{h^2}\right)^{3/2}\exp\left(-\frac{IP_{Cu1}}{kT}\right)$$

$$\frac{x_{Cu2}}{x_{Cu1}} = \frac{1}{n_e}\left(\frac{2\pi m_e kT}{h^2}\right)^{3/2}\exp\left(-\frac{IP_{Cu2}}{kT}\right)$$

$$\frac{x_{He1}}{x_{He0}} = \frac{1}{n_e}\left(\frac{2\pi m_e kT}{h^2}\right)^{3/2}\exp\left(-\frac{IP_{He1}}{kT}\right)$$

$$x_{Cu0} + x_{Cu1} + x_{Cu2} = 1$$

$$x_{He0} + x_{He1} = 1$$

$$x_{Cu1} + 2x_{Cu2} + x_{He1} = x_e$$

where n_e is the total electron density, and the other symbols

have been explained above. These six equations are coupled with the equation for the internal energy density (ρE, see above), and they are solved together to obtain the seven unknowns (x_e (or n_e), x_{Cu0}, x_{Cu1}, x_{Cu2}, x_{He0}, x_{He1} and T), from which the number densities of electrons, Cu^0, Cu^+, Cu^{2+}, He^0 and He^+ can be obtained.

If the plasma is sufficiently intense, the laser radiation will be partially absorbed before it can reach the target. This laser absorption is described in the model by electron–ion and electron–neutral inverse Bremsstrahlung (IB), and the absorption coefficients have been presented in ref. 11. The only difference in the present model is that the He^0 atoms and He^+ ions now also contribute in the IB process, and that their densities should be included in the formulae for the absorption coefficients.

3. Results and discussion

The calculations are performed for a Gaussian shaped laser pulse with 10 ns full-width at half-maximum and peak laser irradiance of 4×10^8 W cm^{-2}. Integrated over the entire pulse, this yields a fluence of 4.24 J cm^{-2}. The laser wavelength was assumed to be 266 nm, and the target reflectivity was taken as 0.34.[11] In the calculations, we follow only one laser pulse.

3.1. Temperature distribution in the target

Fig. 1(a) illustrates the calculated temperature distribution in the target, as a function of time during and after the laser pulse, as a result of the laser–solid interaction, in 1 atm He background gas. Initially, the target temperature is assumed to be 300 K, but it rapidly starts increasing to a maximum value of about 7000 K at nearly 20 ns. Then the target temperature starts to decrease, but this temperature drop is much slower than the temperature rise. Indeed, at 100 ns, the temperature at the surface is still about 1500 K. The temperature is at its maximum at the surface, but due to heat conduction, an elevated temperature is found till almost 10 μm inside the target.

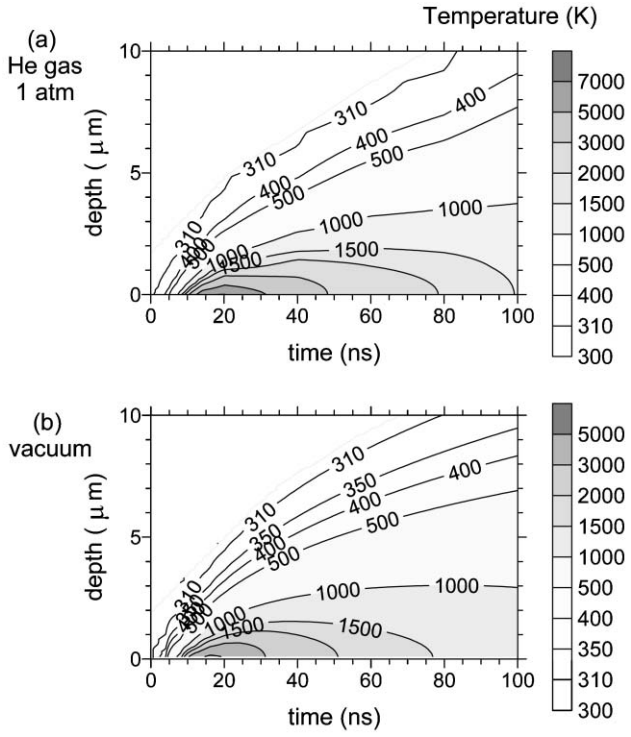

Fig. 1 Calculated temperature distributions in the Cu target, as a function of time during and after the laser pulse, in the case of plume expansion in 1 atm He background gas (a) and for expansion in vacuum (b).

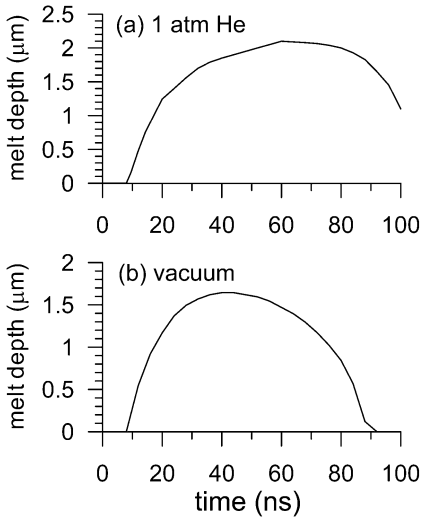

Fig. 2 Calculated melt depth in the Cu target, as a function of time during and after the laser pulse, in the case of plume expansion in 1 atm He background gas (a) and for expansion in vacuum (b).

For comparison, Fig. 1(b) shows the calculated temperature distribution in the target, in the vacuum case. The temperature profile looks very similar, because the mechanisms of heating and heat conduction are the same, but the maximum value is lower (*i.e.*, about 5000 K at the surface, at about 15–20 ns). The reason for this lower target temperature will be explained below (Section 3.6).

3.2. Melt and evaporation depth

As a result of the somewhat higher target temperature in the case of 1 atm He background gas, it is expected that the melt depth and evaporation depth in the target will also be slightly higher than in the vacuum case. This is indeed seen in Figs. 2 and 3. Whereas the melt depth is calculated to be about 2 μm in the case of 1 atm He gas (Fig. 2(a)), it is found to be about 1.6 μm in the vacuum case (Fig. 2(b)). The difference in the depth of evaporation is more significant, as appears from Fig. 3, *i.e.*, about 140 nm in the case of 1 atm He gas (Fig. 3(a)) *versus* about 32 nm in the vacuum case (Fig. 3(b)). The reason for this larger difference is that the evaporation depth is mainly determined by the surface temperature, where the difference

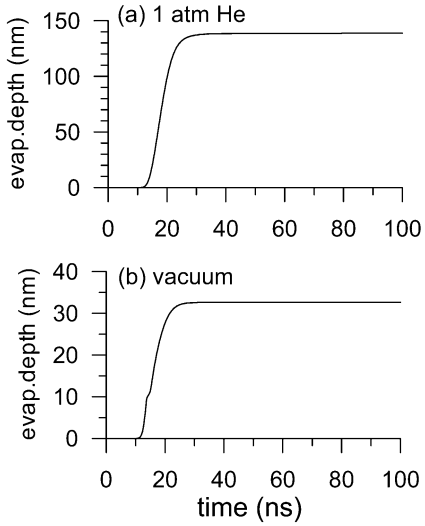

Fig. 3 Calculated evaporation depth in the Cu target, as a function of time during and after the laser pulse, in the case of plume expansion in 1 atm He background gas (a) and for expansion in vacuum (b).

between the case of 1 atm He gas and the vacuum case is quite large (see Fig. 1). Deeper inside the target, there is not so much difference between the temperature for the case of 1 atm He gas and vacuum, which explains why the melt depth is not so different (Fig. 2).

The temporal profiles of the melt and evaporation depths, on the other hand, look quite similar for the case of 1 atm He gas and vacuum. Melting starts to occur at about 10 ns, when the target temperature rises above 1358 K (*i.e.*, the melting point of Cu). The melt depth is at its maximum at about 60 ns in the case of 1 atm He gas, and at 40 ns in the vacuum case. At later times, the target starts to cool down very slowly, and resolidification occurs. Hence, the melt depth (or depth of molten material) drops again. At 100 ns, the melt depth is about 1 μm in the case of 1 atm He gas, whereas in the vacuum case, the target appears to be again completely in solid state at this time.

The depth of evaporation shows a different time-profile compared with the melt depth. The evaporation depth starts rising after about 12 ns, and it increases until about 25–30 ns. Indeed, most evaporation takes place between 12 and 25 ns, when the laser pulse is on. At later times, the evaporation depth remains constant, because the evaporation process has stopped.

In our model, it is assumed up to now that material removal occurs only by evaporation. However, in reality, splashing of molten material due to the recoil pressure of the plume can occur, and this will also contribute to the material removal.[11] The relative importance of the latter mechanism can be deduced from measured crater depths after one laser pulse. Indeed, if we assume that the melt is completely ejected before resolidification occurs, the crater depth would be comparable to the melt depth. For instance, in the book of Ready[18] (Table 3.8, pg. 111), a measured crater depth of 2.2 μm was reported for laser ablation by a 44 ns laser pulse with 10^9 W cm^{-2} irradiance. This value would indeed suggest that for these conditions splashing of molten material is responsible for a great deal of material removal. Therefore, in future work, we intend to include this mechanism in our model. However, since the splashing probably occurs mainly in the radial direction, our one-dimensional model will first have to be extended into two dimensions in order to describe this process in a correct way.

3.3. Effect of the Knudsen layer theory

As discussed above, in Section 2.2, the Knudsen layer theory should be applied in the case of expansion in 1 atm He gas. This Knudsen layer can be seen as a very thin layer (with thickness in the order of a few mean free paths) in front of the target, in which the vapor density and temperature drop by about a factor of 2, as a result of the conservation laws of mass, momentum and energy.[17] At the same time, these conservation equations also affect the flow velocity of the evaporated material.

Fig. 4 shows the calculated flow velocity of the evaporated material at the surface, as a function of time, for the case of expansion in 1 atm He gas, without considering a Knudsen layer (broken line), as well as after applying the Knudsen layer theory (solid line). In case of neglecting the Knudsen layer, the flow velocity varies smoothly as a function of time, and is always positive. However, when the Knudsen layer is taken into account, the flow velocity just outside this layer varies strongly with time. During the laser pulse (*i.e.*, until 30 ns), the flow velocity is positive. After the laser pulse is finished, the flow velocity outside the Knudsen layer, *i.e.*, close to the surface, changes from a positive to a negative value. Indeed, there is more energy loss at the surface (due to heat conduction into the target as well as evaporation) than energy gain (laser energy deposition), which results, according to the Knudsen

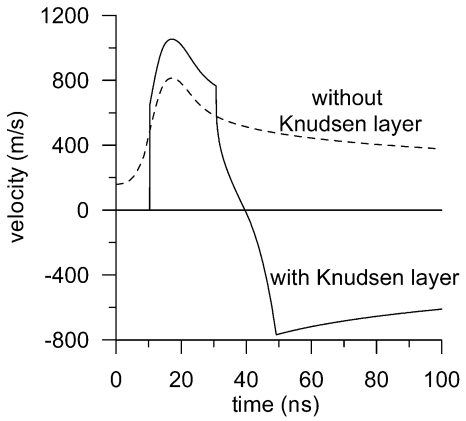

Fig. 4 Calculated flow velocity of the evaporated Cu material as a function of time during and after the laser pulse, in the case of 1 atm He gas, when including (solid line) or neglecting (broken line) Knudsen layer theory.

layer theory, in a negative velocity (see eqn. 15 of ref. 17). From a physical point of view, we can explain this negative velocity because there is not much evaporation any more and, consequently, there is a low vapor pressure in front of the target, resulting in a pressure gradient, and consequently a vapor flow towards the target (see also below). The latter could give rise to the mechanism of liquid splashing, as discussed above.

3.4. Density profiles of evaporated material and background gas

In Fig. 5, the calculated density profiles of the evaporated Cu material and the He background gas are illustrated, at various times. At 20 ns, the vapor density is at a maximum near the target, as a result of evaporation. At later times, the evaporation process has stopped, and the vapor density is spread out due to expansion. The maximum is now lower and shifted away from the target, and the profile becomes broader. As a result of the vapor plume expansion, the He background gas is pushed away from the target, and is piled up just in front of the vapor plume.

For comparison, Fig. 6 shows the calculated density profiles of the evaporated Cu material, at the same times, for expansion in vacuum. The major difference is that the plume is confined to a much smaller region when expanded in a background gas. For instance, at 100 ns, the plume length is calculated to be about 0.3 mm in the case of expansion in the background gas, compared with nearly 2 mm in the vacuum case.

3.5. Velocity and temperature distributions in the plume

Fig. 7 shows the velocity of the plume, as a function of position and at different times. Depending on the position in the plume, the flow velocity can either reach supersonic and subsonic values. As anticipated above, the calculated expansion velocity is much lower for expansion in a background gas compared with expansion in vacuum (*i.e.*, 1000–2000 m s^{-1} *versus* 20 000–25 000 m s^{-1}, as is illustrated in Fig. 7). Indeed, the background gas acts in retarding the plume expansion. Moreover, once evaporation is finished, the plume can move in two directions: (i) away from the target, in the expansion process, but also (ii) towards the target, as a result of the background gas pressure. This is clearly observed in Fig. 7(a). A small negative velocity was also found in the vacuum case, but it is much more pronounced in the case of expansion in the background gas. It is this recoil of the plume that can give rise to splashing of the molten material (see above).

Fig. 8 illustrates the temperature distributions in the plume, at different times, for expansion in the background gas (a) and in vacuum (b). At 20 ns, the temperature is at a maximum near

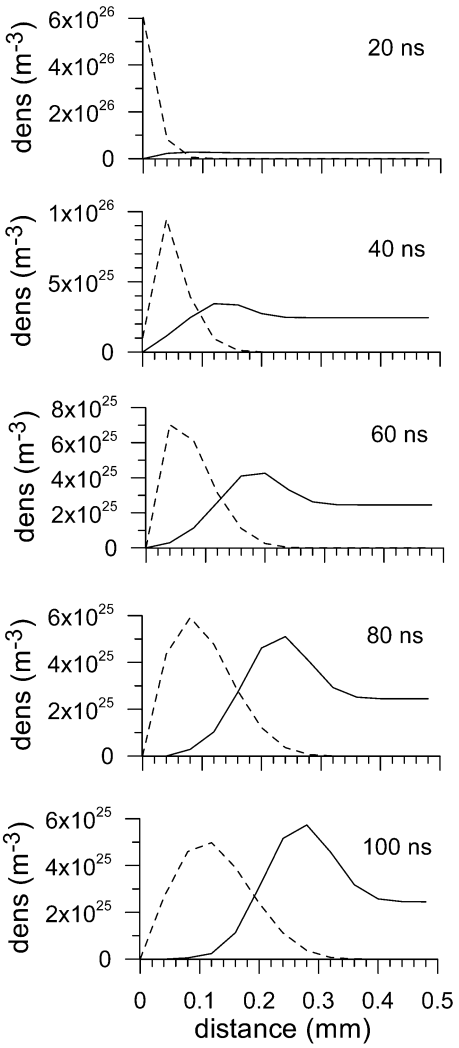

Fig. 5 Calculated density profiles of the evaporated Cu plume (broken lines) and the He background gas (solid lines), at different times, in the case of expansion in 1 atm He gas.

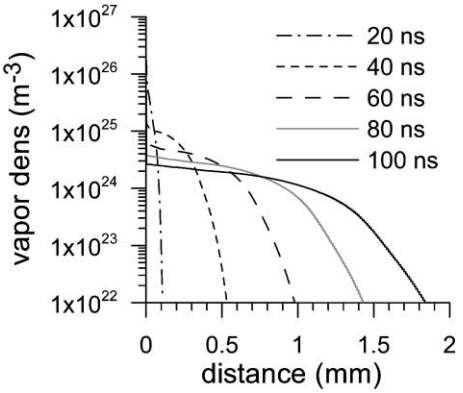

Fig. 6 Calculated density profiles of the evaporated Cu plume, at different times, in the case of expansion in vacuum.

the target, but later on the maximum shifts away from the target, in both cases. It is clear from this figure that the plume temperature is much lower in the case of expansion in the background gas, compared with expansion in vacuum (*i.e.*, order of 2000–3000 K (Fig. 8(a)) *versus* 15 000–25 000 K [Fig. 8(b)]). The main reason is the cooling effect of the background gas, which was initially at room temperature. Another reason is that the ionization degree in the evaporated plume is calculated to be much lower in the case of 1 atm He

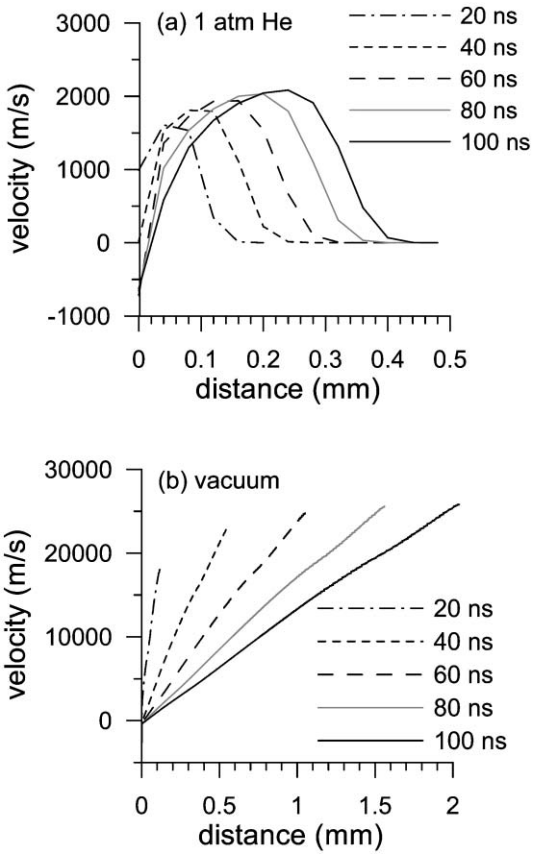

Fig. 7 Calculated expansion velocities of the plume, at different times, in the case of expansion in 1 atm He gas (a) and for expansion in vacuum (b).

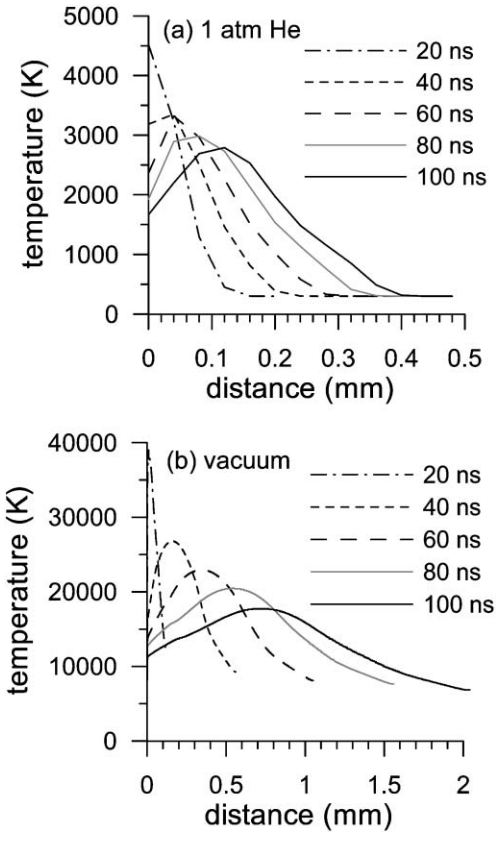

Fig. 8 Calculated temperature distributions in the plume, at different times, in the case of expansion in 1 atm He gas (a) and for expansion in vacuum (b).

gas, compared with the vacuum case (see below), which results in much weaker plasma–laser interaction, and hence in a lower temperature (indeed, laser absorption in the plasma is a heating term in the energy conservation equation; see eqn. 4, in section 2.2). Finally, the third (minor) reason is the temperature jump in the Knudsen layer, in the case of 1 atm He gas (see above; section 3.3). In the vacuum case, this Knudsen layer theory was not applied, because it is mainly important for high background gas pressure.

3.6. Ionization degree in the Cu plume, and plasma formation

As a result of the much lower plume temperature in the case of expansion in the background gas, plasma formation is calculated to be far less important compared with the vacuum case.[11] In the case of expansion in the background gas, the electron and ion densities were calculated to be around 10^{18}–10^{19} m^{-3}, which corresponds to an ionization degree of only 10^{-7}. For comparison, the density of electrons, Cu^{+} and Cu^{2+} ions in the vacuum case was calculated to be in the order of 10^{25}–10^{26} m^{-3} at 20 ns, and the fractions of Cu^{+} ions, Cu^{2+} ions and electrons are found to be around 0.6, 0.35 and 1.3, respectively. The fraction of Cu^{0} atoms was only of the order of a few %. Hence, our model predicts that, for a laser irradiance of 4×10^{8} W cm^{-2}, in the vacuum case, the Cu plume is nearly fully ionized (and even Cu^{2+} ions are formed), whereas in the case of expansion in 1 atm He gas, only a very weak plasma is formed.

As a result of this low electron density, calculated in the case of 1 atm He gas, plasma–laser interaction, *i.e.*, inverse Bremsstrahlung absorption of the laser beam, is found to be not important under the conditions investigated, and the plasma shielding is, therefore, calculated to be negligible for expansion in the background gas. For expansion in vacuum, on the other hand, plasma–laser interaction, and hence plasma shielding, was calculated to be significant at the conditions under study (*i.e.*, laser irradiance of 4×10^{8} W cm^{-2}). This is, indeed, apparent from Fig. 9, where the solid line shows the laser irradiance, and the broken line depicts the irradiance at the target, after passing through the plasma, in the vacuum case. Note that in the case of 1 atm He gas, the laser irradiance at the target is the same as the initial laser irradiance, *i.e.*, represented by the solid line.

This higher laser irradiance at the target, in case of 1 atm He gas, explains why the calculated target temperature was higher in the case of the background gas, compared with the vacuum case (see above, Fig. 1).

Nevertheless, it should be mentioned that for higher laser irradiance, the process of laser–plasma interaction quickly becomes important in the case of expansion in the background gas. However, we believe that the present model is not yet realistic for these higher values of laser irradiance, because the plume temperature then rises drastically, and the plasma shielding due to electron–neutral inverse Bremsstrahung is significant, because of the very high neutral density at 1 atm. This high degree of plasma–laser interaction, and consequently the high temperature, is probably an overestimation of the one-dimensional model, *i.e.*, the energy cannot be spread out in the radial direction. Moreover, some other energy loss processes, such as excitation, should be incorporated in the model. We hope that this problem will be solved when extending the model into two dimensions, and when extra energy loss mechanisms (such as excitation) are taken into account. We plan to carry out these modifications to the model in the near future.

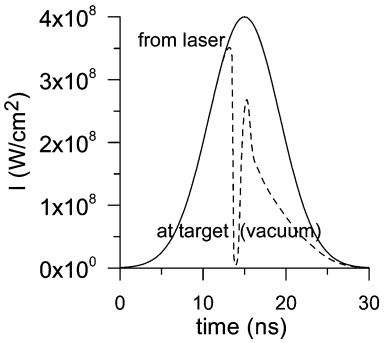

Fig. 9 Laser irradiance–time profile, assumed in the model (solid line), both for expansion in 1 atm He gas and in the vacuum case. The broken line illustrates the laser irradiance at the target, *i.e.*, after passing through the vapor plume (plasma), in the vacuum case. In the case of expansion in 1 atm He, the laser irradiance at the target was found to be the same as the original laser irradiance (solid line, no plasma shielding).

4. Conclusion

We have developed a numerical model for the interaction between a ns-pulsed laser and a Cu target, and the expansion of the evaporated Cu material in 1 atm He gas. The calculation results, such as target temperature, melt and evaporation depth, density, velocity and temperature profiles in the plume, and ionization degree in the plasma, are shown, and compared with the case of expansion in vacuum.

The major influence of the He background gas is the spatial confinement of the vapor plume, the retardation of the expansion velocity, and the lowering of the plume temperature. As a result, the calculated ionization degree is much lower, for the conditions under investigation (*i.e.*, laser irradiance of 4×10^{8} W cm^{-2}), yielding almost no plasma shielding and hence a higher laser irradiance at the target. The latter results in a somewhat higher target temperature, melt depth and evaporation depth, compared with the vacuum case.

It should, however, be mentioned that the observed differences in plume temperature, plasma formation and laser–plasma interaction, apply to the laser irradiance of 4×10^{8} W cm^{-2}, and may not be generalized to higher values of laser irradiance. Indeed, our model for laser ablation in 1 atm He gas predicts a significant increase in plume temperature, plasma formation (ionization degree) and laser–plasma interaction for higher laser irradiance, which is probably not realistic. For instance, for a laser irradiance of 10^{9} W cm^{-2}, the plasma shielding was calculated to be so important that virtually no laser light could reach the target. Since this value of laser irradiance is quite common in LA work for ICP-MS, this suggests that it yields sufficient material removal, and that the plasma shielding, as predicted with the model, is too high. This could be attributed either to the one-dimensional nature of the model (because it cannot describe energy loss in the radial direction), or to limitations in the model (*e.g.*, no excitation incorporated) or in the solution method for the conservation equations of the expansion dynamics. We hope to solve this problem in the near future (*e.g.*, by extending the model to two dimensions, and by incorporating other energy loss mechanisms, such as excitation), so that the model can be applied to higher values of laser irradiance as well.

Moreover, in future work, we would also like to include the mechanisms in our model that lead to particle formation as a result of laser–solid interaction, *i.e.*, small (nm-sized) particles as a result of condensation due to the cooling of the expanding vapor plume, and larger (μm-sized) particles as a result of direction ejection from the target (*e.g.*, liquid splashing).

Acknowledgements

This work is financially supported by the Flemish Fund for Scientific Research (FWO) and by the Federal Services for Scientific, Technical and Cultural Affairs of the Prime Minister's Office, through IUAP-V. The authors also thank

A. Vertes, S. Mao, N. Bulgakova and R. Gijbels for the interesting discussions and useful advice, and A. Vertes for supplying the original model for laser ablation with expansion in vacuum.

References

1 *Pulsed Laser Deposition of Thin Films*, eds. D. B. Chrisey and G. K. Hubler, Wiley, New York, 1994.
2 M. F. Becker, J. R. Brock, H. Cai, D. E. Henneke, J. W. Keto, J. Lee, W. T. Nichols and H. D. Glicksman, *NanoStruct. Mater.*, 1998, **10**, 853.
3 S. Ameer-Beg, W. Perrie, S. Rathbone, J. Wright, W. Weaver and H. Champoux, *Appl. Surf. Sci.*, 1998, **127–129**, 875.
4 F. H. Loesel, J. P. Fischer, M. H. Götz, C. Horvath, T. Juhash, F. Foack, N. Suhm and F. J. Bille, *Appl. Phys. B*, 1998, **66**, 121.
5 M. C. Galicia, A. Vertes and J. H. Callahan, *Anal. Chem.*, 2002, **74**, 1891.
6 L. J. Radziemski, *Spectrochim. Acta, Part B*, 2002, **57**, 1109.
7 R. E. Russo, *Appl. Spectrosc.*, 1995, **49**, 14A.
8 D. Günther, S. E. Jackson and H. P. Longerich, *Spectrochim. Acta, Part B*, 1999, **54**, 381.
9 R. E. Russo, X. Mao and S. S. Mao, *Anal. Chem.*, 2002, **74**, 70A.
10 D. Günther, B. Hattendorf and C. Latkoczy, *Anal. Chem.*, 2003, **75**, 341A.
11 A. Bogaerts, Z. Chen, R. Gijbels and A. Vertes, *Spectrochim. Acta, Part B*, 2003, **58**, 1867.
12 A. G. Gnedovets, A. V. Gusarov and I. Smurov, *J. Phys. D: Appl. Phys.*, 1999, **32**, 2162.
13 A. G. Gnedovets, A. V. Gusarov and I. Smurov, *Appl. Surf. Sci.*, 2000, **154–155**, 508.
14 A. V. Gusarov, A. G. Gnedovets, I. Smurov and G. Flamant, *Appl. Surf. Sci.*, 2000, **154–155**, 331.
15 R. B. Bird, W. E. Steward and E. N. Lightfoot, *Transport Phenomena*, Wiley, New York, 1960.
16 C. Hirsch, *Numerical Computation of Internal and External Flows*, Wiley, New York, 1990, vol. 2.
17 C. J. Knight, *AIAA J.*, 1979, **17**, 519.
18 J. F. Ready, *Effects of High Power Laser Radiation*, Academic Press, New York, 1971.